Program Digest, 2019 IEEE International Ultrasonics Symposium (IUS)
Glasgow, Scotland, October 6-9, 2019

2-D Shear wave dispersion images using the reverberant shear wave field approach: application in tissues exhibiting power law response

Juvenal Ormachea*, Richard G. Barr†, and Kevin J. Parker*,
*Department of Electrical and Computer Engineering, University of Rochester, Rochester, NY, USA
†Department of Radiology, Northeastern Ohio Medical University, Youngstown, OH, USA

***Abstract*—Within the field of elastography, a relatively new approach analyzes the limiting case of shear waves established as a reverberant field. In this framework, it is assumed that a distribution of shear waves exists, oriented across all directions in 3D and continuous in time. The simultaneous multi-frequency application of reverberant shear wave fields can be accomplished by applying an array of external sources that can be excited by multiple frequencies, for example 50, 100, 150,...500 Hz, all contributing to the shear wave field produced in the target organ. We report a Monte Carlo analysis simulation for the validation of the main theoretical principles, and a preliminary study on breast and liver tissues using the multi-frequency reverberant shear wave technique, employing frequencies up to 700 Hz in breast tissue, and robust reverberant patterns of shear waves across the entire liver and kidney in obese patients. Dispersion images are shown to have contrast between tissue types and with quantitative values that align with previous studies.**

***Index Terms*—reverberant shear wave field, shear dispersion, shear elastography, deep tissue viscoelasticity**

I. Introduction

Parker et al. [1] proposed and analyzed a fully reverberant shear wave elastography (R-SWE) field produced by sending continuous harmonic shear wave excitations to tissue. This approach had been evaluated and compared with another well-known elastography technique in different calibrated phantoms [2], *in vivo* liver and breast tissues using an ultrasound-based method [2], and in *ex vivo* pig cornea using an optical-based method [3]. In Ormachea et al. [2], the R-SWE approach was applied using individual and multi-vibration frequencies, obtaining similar shear wave speed (SWS) results for both types of experiments. This enables the analysis of the dispersion of SWS as it increases with frequency, indicating the viscoelastic and lossy nature of the tissue under study. Thus, the multi-frequency approach presents some advantages: it can more quickly assess the biomechanical tissue properties by estimating the SWS and dispersion, and the data is collected at the same time for different frequencies, which facilitates its use for clinical applications. Furthermore, dispersion images can be created and displayed alongside the SWS images. In this work, a Monte Carlo analysis simulation was conducted for the validation of the main theoretical principles, then two different calibrated CIRS phantoms, three *in vivo* livers, and two *in vivo* breast tissues were scanned as an initial study for 2-D dispersion images using the R-SWE approach.

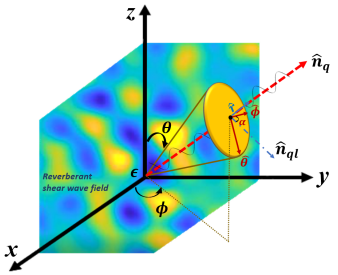

Fig. 1. Schematic for an object that has an isotropic random distribution of shear waves propagating through the interior, consistent with the theory of reverberant fields [3].

II. Theory

A. Reverberant shear wave field

For a given point $\boldsymbol{\epsilon}$ in the cartesian system, three orthogonal vectors in the spherical coordinate system are found: $\hat{\mathbf{r}}$, $\hat{\boldsymbol{\theta}}$, and $\hat{\boldsymbol{\phi}}$. Then, the corresponding particle velocity vector field $\mathbf{V}(\boldsymbol{\epsilon}, t)$, at position $\boldsymbol{\epsilon}$ and time t, in a reverberant chamber produced by plane waves propagating with a wave number k and radial frequency ω_0 is modeled as

$$\mathbf{V}(\boldsymbol{\epsilon}, t) = \sum_{q,l} \hat{\mathbf{n}}_{ql} v_{ql} e^{i(k\hat{\mathbf{n}}_q \cdot \boldsymbol{\epsilon} - \omega_o t)} \tag{1}$$

where the index q represents a realization of the random unit vector $\hat{\mathbf{n}}_q$ describing the direction of wave propagation, and the index l represents a realization of the random unit vector $\hat{\mathbf{n}}_{ql}$ describing direction of particle velocity parallel to the disk formed by the basis vectors $\hat{\boldsymbol{\theta}}$ and $\hat{\boldsymbol{\phi}}$ (See Figure 1 following the reference [3]) defined within a realization of q. Then, $\hat{\mathbf{n}}_q \cdot \hat{\mathbf{n}}_{ql} = 0$. Finally, v_{ql} is an independent, identically-distributed random variable describing the magnitude of particle velocity within a realization of q. The summation over q is understood to be taken over the 4π solid angle, and the summation over l is taken over a 2π angle within the disk.

In order to solve the autocorrelation function B_{vv} of eqn (1), two cases were considered: the autocorrelation direction perpendicular, and parallel to the axis where the system measures the particle velocity.

$$B_{v_z v_z}(\Delta\boldsymbol{\epsilon}, \Delta t) = \frac{\beta}{2} e^{i\omega_0 \Delta t} \cdot \left[j_0(k\Delta\boldsymbol{\epsilon}_x) - \frac{j_1(k\Delta\boldsymbol{\epsilon}_x)}{k\Delta\boldsymbol{\epsilon}_x} \right] \quad (2)$$

$$B_{v_z v_z}(\Delta\boldsymbol{\epsilon}_z, \Delta t) = \frac{\beta}{2} e^{i\omega_0 \Delta t} \cdot \frac{j_1(k\Delta\boldsymbol{\epsilon}_z)}{\Delta\boldsymbol{\epsilon}_z} \quad (3)$$

where j_0 and j_1 are spherical Bessel functions of the first kind of zero and first order, respectively, and the spatial and temporal components of $B_{v_x v_x}(\Delta\boldsymbol{\epsilon}, \Delta t)$ are separable.

B_{vv} is calculated and fit to eqn (2) or (3) to estimate the unknown parameter k. Local estimates of k are used to create a map, typically displayed in color, representing the SWS, a measure of the stiffness of the tissue, at different locations.

B. 2-D linear dispersion slope (LDS) and power law coefficient (PLC) estimation.

In Parker et al. [4], it was shown that some viscoelastic phantoms and soft tissues exhibit a power law response. In these cases, the phase velocity can be written as:

$$c_s = c_1 \omega^a \quad (4)$$

where c_1 is the phase velocity measured at angular frequency $\omega = 1$ rad/s, and a is the power law coefficient. Frequently the simplest measurement of dispersion is the linear slope ($dc_s/d\omega$). However, this parameter has been found in tissues to vary strongly as a function of frequency. Considering a power law media, a simplification results if one plots c_s versus ω data on a log–log scale. In other words, the slope or dispersion as measured from a log–log plot of c_s versus ω will be constant across different frequency bands. Our multi-frequency data are analyzed for both the traditional linear (slope) dispersion and for power law dispersion by performing a linear regression fitting.

III. Methods

A. Ultrasound scanner, data acquisition, and vibration sources

A Verasonics ultrasound system (Vantage-128TM, Verasonics, Kirkland, WA, USA), connected to a convex ultrasound probe (model C4-2, ATL, Bothell, WA, USA) or a linear ultrasound probe (model L7-4, ATL, Bothell, WA, USA) were used to track the induced displacements. The linear probe was used for the breast phantom and breast tissue applications, whereas the convex probe was used for deeper scans in the viscoelastic phantom and liver tissue. The center frequencies were 3 MHz and 5 MHz for the convex and linear probes, respectively. The tracking pulse repetition frequency (PRF) was set to 3600 Hz with a total acquisition time of 0.5 seconds. A custom-made portable trifold futon ($70 \times 60 \times 10$ cm^3) with multiple embedded vibration sources (Quad Resonator Model EI718 TM, Elastance Imaging LLC, Columbus, OH, USA) was mounted to a clinical bed to generate the reverberant shear wave field.

TABLE I
Summary of Monte Carlo analysis

	a	Frequency (Hz)			LDS (m/s/100Hz)	PLC
		100	300	500		
Eqn. 4	0.125	1.16	1.31	1.38	0.05	0.125
R-SWE	0.125	1.05±0.14	1.26±0.04	1.36±0.04	0.08±0.02	0.16±0.06
Eqn. 4	0.24	2.26	2.90	3.26	0.20	0.24
R-SWE	0.24	1.95±0.75	2.88±0.25	3.22±0.17	0.22±0.08	0.26 ±0.11

B. Monte Carlo analysis

Similar to [3], a 25×25×25 mm^3 field ($\Delta x = \Delta y = \Delta z = 0.3$ mm sampling resolution) is generated in MATLAB (The MathWorks, Inc. Natick, MA, USA). Evaluating eqn 1, a single plane and shear wave is defined by uniformly-distributed random variables of $\hat{\mathbf{n}}_{\mathbf{q}}$, $\hat{\mathbf{n}}_{ql}$, and $\mathbf{v}_{ql}$. A total of 20,000 realizations of all random variables generates a spatial and complex-valued particle velocity vector field $\mathbf{V}(\boldsymbol{\epsilon})$, where $\mathbf{V}(\boldsymbol{\epsilon}, t) = \mathbf{V}(\boldsymbol{\epsilon}) e^{-i\omega t}$, and $\omega = 2\pi f$ with $f = 50$ to 500 Hz. The wave number is defined as $k(\omega) = \omega / c_s$ in the entire field.

C. CIRS phantoms and in vivo tissue

A homogeneous part (20 kPa nominal Young's modulus) from the background region of the CIRS breast phantom (Model 059, Computerized Imaging Reference Systems, Norfolk, VA, USA) was chosen to evaluate R-SWE. Then, a custom made CIRS (Serial No. 2095.1-1, Computerized Imaging Reference Systems) homogeneous viscoelastic phantom (6 kPa nominal Young's modulus) was chosen to evaluate R-SWE. Five healthy volunteer patients were scanned to evaluate the feasibility of applying the R-SWE modality in *in vivo* experiments. One thin and two obese patients were scanned for the *in vivo* liver experiments. Two patients, one with a breast fibroadenoma and one with dense breast tissue, were scanned for breast experiments. During the experiments, the patients reclined supine on the custom bed. These scans were conducted under the requirements of informed consent of the Southwoods Imaging Clinical Institutional Review Board.

IV. Results

The Monte Carlo analyses were conducted considering two different a values in eqn 4 (i.e. 0.125 and 0.24) with $c_1 = 0.45$ m/s. For each simulation, the SWS was measured using the R-SWE approach and then, LDS and PLC images were obtained using eqn 4. Figure 2 shows the SWS at 400 Hz, the LDS, and the PLC images for the two a cases. Figure 3 shows a comparison plot of SWS as a function of frequency, using eqn 4 and the R-SWE results for the simulated data. Table I reports the SWS theoretical values using eqn 4, the measured LDS, and PLC. It also shows the estimated results using the R-SWE results at different frequencies and the estimated LDS and PLC for the two a cases.

Figure 4 shows the SWS, LDS, and PLC maps superimposed on their corresponding B-mode images for the vis-

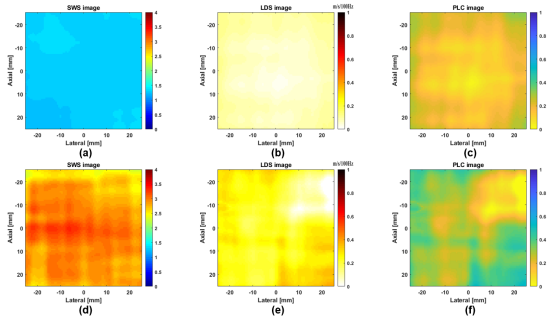

Fig. 2. (Top row (left to right), estimated, SWS, LDS, and PLC images for case a =0.125. Bottom row (left to right), estimated, SWS, LDS, and PLC images for case a =0.24.

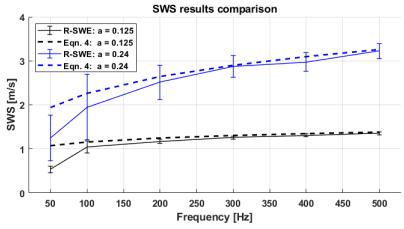

Fig. 3. Comparison SWS versus frequency plots for the Monte Carlo analysis using a =0.125 (blue) and a =0.24 (black). Higher dispersion was obtained for the second case (a =0.24) as expected. Mean and SD values were extracted for same ROI sizes in all SWS images.

TABLE II
SUMMARY OF VISCOELASTIC MATERIAL PROPERTIES IN DIFFERENT MEDIA

Media (Hz)	SWS (m/s)	LDS (m/s/100Hz)	PLC	Frequency range (Hz)	R^2 LDS	R^2 PLC
Breast phantom	2.15±0.11	0.10±0.02	0.18±0.11	200-500	0.77±0.14	0.73±0.12
Viscoelastic phantom	1.88±0.38	0.42±0.02	0.34±0.03	80-320	0.73±0.05	0.71±0.07
Liver 1, thin patient	1.99±0.19	0.28±0.14	0.23±0.10	80-320	0.92±0.05	0.90±0.07
Liver 2, obese patient	2.29±0.37	0.49±0.17	0.44±0.09	80-320	0.82±0.14	0.80±0.12
Liver 3 obese patient	2.38±0.20	0.54±0.19	0.43±0.04	80-320	0.75±0.14	0.72±0.17
Breast 1, fibroadenoma	3.71±0.29	0.29±0.04	0.54±0.3211	468-702	0.72±0.09	0.75±0.11
Breast 2, dense breast tissue	4.33±0.34	0.48±0.15	0.58±0.21	468-702	0.96±0.12	0.95±0.17

coelastic phantom. Figure 5 shows a reference plot of SWS, extracted for a region of interest (ROI), as a function of frequency for both phantoms. As expected, the SWS remained nearly constant for the breast phantom since it is a nearly elastic material. On the other hand, the SWS increased with an increasing frequency for the viscoelastic phantom.

Figure 6 show the different viscoelastic images for a obese patient. The liver is located 4 – 10 cm depth in Figure 6. Thus, R-SWE was able to measure the viscoelastic properties of liver tissue in obese patients at deep regions. Additionally, it can be observed that the kidney was also measured in Figure 6. For this case, a simple observation at 200 Hz shows a clearer distinction between the kidney cortex and the liver tissue.

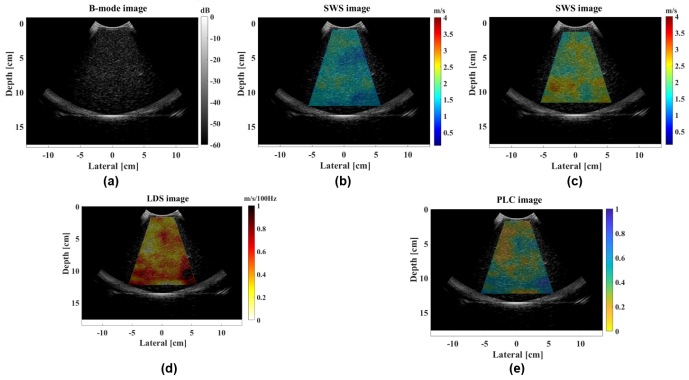

Fig. 4. (a) B-mode images for the CIRS viscoelastic phantom, (b-c) SWS images, superimposed on their corresponding B-mode image, obtained with the R-SWE approach at two different vibration frequencies, 80 Hz and 200 Hz, respectively. (d-e) LDS and PLC images using a 80 – 320 Hz frequency range.

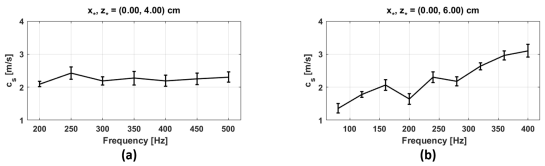

Fig. 5. SWS versus frequency plots for the CIRS breast (a) and viscoelastic phantoms (b). Higher dispersion was obtained for the viscoelastic media.

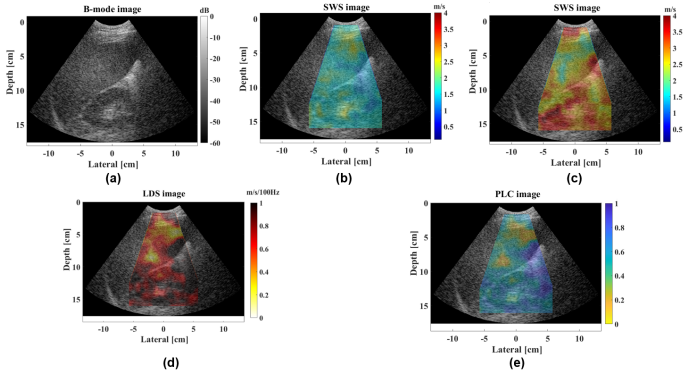

Fig. 6. (a) B-mode images for Patient #3 (liver obese case), (b-c) SWS images, superimposed on their corresponding B-mode image, obtained with the R-SWE approach at two different vibration frequencies, 80 Hz and 200 Hz, respectively. (d-e) LDS and PLC images using a 80 – 320 Hz frequency range.

Although this suggests that R-SWE may be able to measure the viscoelastic properties in kidney tissue, further research is needed with more focus in this organ. Both obese patients show higher LDS and PLC results than the thin patient's liver (see Table II for details). Figure 7 shows a reference plot of SWS, extracted for a ROI, as a function of frequency for the obese liver tissue cases.

Figure 8 shows the breast experiment with the benign fibroadenoma. The SWS maps illustrate the presence of the lesion that has a lower SWS than the surrounding tissue. The

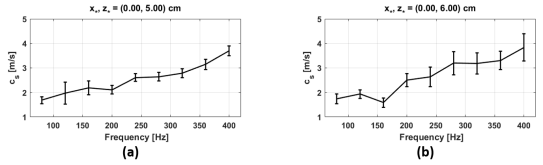

Fig. 7. SWS versus frequency plots for Patient #2's liver (a) and Patient #3's liver (b).

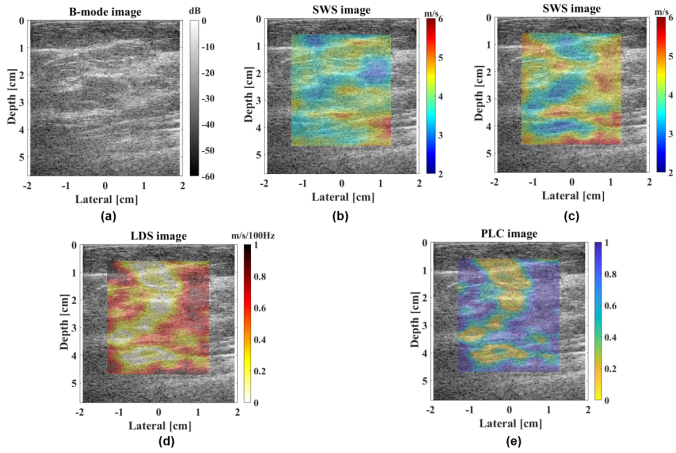

Fig. 8. (a) B-mode images for Patient #4 (breast fibroadenoma case), (b-c) SWS images, superimposed on their corresponding B-mode image, obtained with the R-SWE approach at two different vibration frequencies, 585 Hz and 702 Hz, respectively. (d-e) LDS and PLC images using a 468 – 702 Hz frequency range.

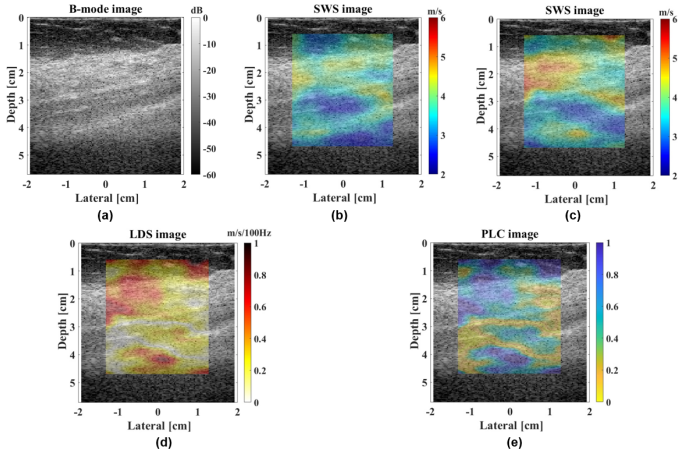

Fig. 9. (a) B-mode images for Patient #5 (dense breast tissue case), (b-c) SWS images, superimposed on their corresponding B-mode image, obtained with the R-SWE approach at two different vibration frequencies, 585 Hz and 702 Hz, respectively. (d-e) LDS and PLC images using a 468 – 702 Hz frequency range.

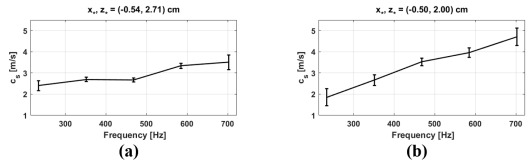

Fig. 10. SWS versus frequency plots for Patient #4's breast (a) and Patient #5's breast (b).

SWS value was lower than benign masses reported in Barr et al. [5]. Figure 9 shows the viscoelastic results for the dense breast tissue experiment. Figure 10 shows a reference plot of SWS, extracted for a ROI, as a function of frequency for both breast tissue cases. Additionally, the goodness of the curve fit, represented by the R^2 value, is also reported for all the LDS and PLC results in Table II.

V. Conclusion

The Monte Carlo analysis validates the main theoretical principles related with the R-SWE approach to measure the SWS and dispersion properties in different viscoelastic media. This proof of concept study demonstrates that reverberant shear wave fields can be produced in deep tissues from external sources, up to 400 Hz in obese patients' livers and over 700 Hz in breast tissue. The dispersion can be analyzed as a slope or as a power law coefficient consistent with a more advanced framework of tissue rheology. These dispersion properties are then measured over an entire ROI and used to form dispersion images. These may provide additional information and image contrast in cases where lesions or pathologies show an altered viscoelastic response, and therefore an altered dispersion parameter, compared with normal tissue. Further study is required to define the practical upper limits to shear wave frequencies applied to the breast or liver within our framework, and the range of normal dispersions expected within a healthy population.

Acknowledgment

Juvenal Ormachea was supported by Peruvian Government scholarship 213-2014-FONDECYT. This work was supported by the Hajim School of Engineering and Applied Sciences at the University of Rochester. We are grateful to Elastance Imaging for the loan of their Quad Resonator.

References

[1] K. J. Parker, J. Ormachea, F. Zvietcovich, and B. Castaneda, "Reverberant shear wave fields and estimation of tissue properties," Physics in Medicine & Biology, vol. 62, no. 3, p. 1046, 2017.
[2] J. Ormachea, B. Castaneda, and K. J. Parker, "Shear wave speed estimation using reverberant shear wave fields: Implementation and feasibility studies," Ultrasound in medicine & biology, vol. 44, no. 5, pp. 963–977, 2018.
[3] F. Zvietcovich, P. Pongchalee, P. Meemon, J. P. Rolland, and K. J. Parker, "Reverberant 3D Optical Coherence Elastography maps the elasticity of individual corneal layers," Nature Communications (Accepted), 2019.
[4] K. J. Parker, J. Ormachea and Z. Hah , "Group versus Phase Velocity of Shear Waves in Soft Tissues", Ultrason Imaging, 40 343-56, 2018.
[5] R. G. Barr, K. Nakashima, D. Amy, D. Cosgrove, A. Farrokh, F. Schafer, J. C. Bamber, L. Castera, B. I. Choi, Y.-H. Chou et al., "Wfumb guidelines and recommendations for clinical use of ultrasound elastography: Part 2: breast," Ultrasound in medicine & biology, vol. 41, no. 5, pp. 1148–1160, 2015.